Conduction Mechanism of Aviram−Ratner Rectifiers with Single Pyridine−σ−C_{60} Oligomers

Bing Wang,* Yunshen Zhou, Xunlei Ding, Kedong Wang, Xiaoping Wang, Jinlong Yang, and J. G. Hou*

Hefei National Laboratory for Physical Sciences at Microscale, University of Science and Technology of China, Hefei, Anhui 230026, People's Republic of China

Received: August 7, 2006; In Final Form: September 29, 2006

We present the electron transport of pyridyl aza[60]fulleroid oligomers, abbreviated as C_{60}NPy, which is based on the donor−barrier−acceptor (D−σ−A) architecture, at a single molecular scale using scanning tunneling microscopy. A rectifying effect is observed in the current−voltage characteristics. The theoretical calculation shows that the highest occupied molecular orbital (HOMO) and the lowest unoccupied molecular orbital (LUMO) are well localized either on the Py moiety (donor) or on the C_{60} moiety (acceptor), indicating the σ-bridge decouples the LUMO and the HOMO of the donor and the acceptor, respectively. This structure accords well with the unimolecular rectifying model proposed by Aviram and Ratner [*Chem. Phys. Lett.* **1974**, *29*, 277]. The mechanism of the rectifying effect is understood by analyzing in detail the electron transport through energy levels of the donor and the acceptor of the C_{60}NPy molecules. By directly comparing the experimental conductance peaks and the calculated density of states of the C_{60}NPy, we find that the observed rectification is attributed to the asymmetric positioning of the LUMOs and the HOMOs of both sides of the acceptor and the donor of the C_{60}NPy molecules with respect to the Fermi level of the electrodes. When a main voltage drop is over the molecule−electrode vacuum junction but a small fraction over the molecule itself, the shift of the energy levels between the donor and the acceptor will be small. This behavior deviates from the original proposal by Aviram and Ratner in which a large shift of the energy level is expected.

Introduction

Molecular rectifiers have attracted wide attention since the first proposal of the donor−barrier−acceptor (D−σ−A) architecture by Aviram and Ratner (AR).[1] In recent years, molecular rectifiers have been demonstrated either in single molecules[2−6] or in molecular films.[7−14] According to the processes for the rectification, these rectifiers may be classified into three types:[15] (i) based on Schottky barriers at the metal−organic film interfaces,[13] (ii) based on geometrically asymmetric contacts of molecular junctions,[7,8,14,16] and (iii) based on asymmetric positioning of the molecular orbitals with respect to the Fermi level of the electrodes (FLE), i.e., unimolecular rectifiers.[2,3,5,9,11,12,16,17] In the unimolecular rectifiers, the AR model is the most attractive one since it is promising and suitable for molecular engineering.[15]

Though the original AR proposal of D−σ−A is based on the use of a single molecule,[1] where σ is a saturated covalent bridge, most of the studies have been concentrated on molecular junctions with D−π−A molecular films,[4,6−9,13,14,17−21] where π is a conjugated bridge, and only a very few studies have been performed in molecular junctions with D−σ−A films.[10,11,22,23] The conduction mechanism for the rectification in these systems is still a subject of controversy. The analysis by Krzeminski et al. indicates that the π-bridge does not sufficiently isolate D and A to keep molecular orbitals localized on either D or A,[16] and then a D−π−A molecule is unlikely to implement the AR mechanism. Krzeminski et al. attributed the observed rectification in Langmuir−Blodgett films of γ-hexadecylquinolinium tricyanoquinodimethanide to an asymmetric profile of the electrostatic potential. Some theoretical results suggest that there is no rectification or even rectification at the opposite direction.[24−28] For instance, Stokbro et al. argued that it is necessary for molecules to have a much smaller gap of the highest occupied molecular orbital and the lowest unoccupied molecular orbital (HOMO−LUMO) to generate rectification,[28] and Mujica et al. argued that if the voltage drop occurs completely at the molecule−electrode interfaces, the molecular rectification in tunneling junctions is difficult to achieve.[24] It is also noted that in the original AR rectifiers the shift of the energy levels is also involved between the donor and the acceptor under applied voltages.[1] However, in most of the previously studied molecules with D−σ−A or D−π−A there were long alkyl or alkanethiolate tails connected to electrodes.[4,15,18−20] In general, a conjugated molecule is more conductive than a saturated molecule of the same length.[29] Hence, in a system of D−σ−A or D−π−A tailored with alkyl chains the main voltage is expected to drop over the tailored chains, but only a small fraction over the D−σ−A or D−π−A group itself, causing a small shift of the energy levels between the D and the A part. In such a situation, the mechanism of the rectification is different from the original model of AR rectifiers; then what are the detailed processes for the current flow along the long chain tailored D−σ−A or D−π−A molecules?

To clarify and answer the questions above requires insight into the conduction mechanism of AR rectifiers based on analyzing the electron transport through molecular orbitals and, thus, requires an investigation at a single molecular scale. To the best of our knowledge, up to now, there has been no

* To whom correspondence should be addressed. E-mail: bwang@ustc.edu.cn (B.W.); jghou@ustc.edu.cn (J.G.H.).

10.1021/jp065069t CCC: $33.50
Published on Web 11/11/2006

SCHEME 1: Synthesis of *N*-3-γ-Pyridyl Aza[60]fulleroid (C_{60}NPy)

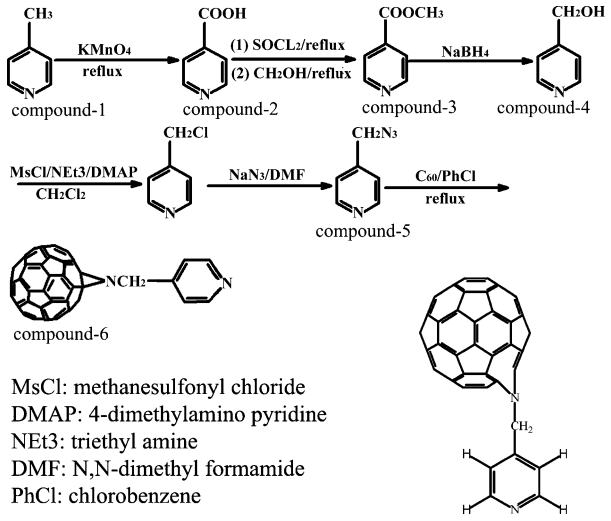

experimental realization of AR rectification at a single molecular scale. The details of the electron transport between the orbitals of the D$-\sigma-$A or D$-\pi-$A molecules are not clear since one still lacks experimental data for comparing directly with theoretical results.

The purpose of this paper is to investigate the conduction mechanism of AR rectifiers at a single molecular scale with a designed D$-\sigma-$A molecule, directly comparing experimental data with theoretical calculations. *N*-3-γ-Pyridyl aza[60]fulleroid (abbreviated as C_{60}NPy), with a D$-\sigma-$A structure, was synthesized and studied with scanning tunneling microscopy/spectroscopy (STM/STS) performed at low temperatures of 78 and 5 K. The asymmetric current$-$voltage ($I-V$) characteristic, i.e., molecular rectification, was observed. The conductance peaks in the dI/dV spectra obtained at 5 K are compared with the electronic structure calculated by density-functional theory (DFT). The conduction mechanism is analyzed for the electron transport between the molecular orbitals of the C_{60} moiety and the ones of the pyridine moiety. The results show that the dI/dV spectra reflect in part the electronic structure of the molecule, which gives a clue for understanding the electron transport through the D$-\sigma-$A molecule. The role of the vacuum gap between the STM tip and the molecule is also discussed.

Experimental Section

C_{60}NPy Molecules. C_{60}NPy molecules were obtained via cycloaddition reaction of 4-azidomethylpyridine to C_{60}, as illustrated in Scheme 1.[30−33] (See the Supporting Information.)

STM/STS Sample Preparation. Several pieces of gold (111) thin films on mica were immersed into toluene solutions of pure C_{60}NPy (CP-SAM), pure benzyl mercaptan (BM-SAM), and mixtures of BM and C_{60}NPy with mole ratios of 100:1 (co-SAM-1) and 1:30000 (co-SAM-2), respectively, for about 48 h.[34] The samples were annealed at 55 and 105 °C in a vacuum. The BM molecules could be thoroughly desorbed after the samples were annealed at 105 °C for about 10 h. Both the as-grown and the annealed samples were transferred to the cryostat of a low-temperature scanning tunneling microscope (LTSTM, Omicron SCALA) precooled to 77 or 5 K for STM/STS measurements without breaking the vacuum. The $I-V$ characteristics were measured by turning off the feedback loop of the microscope.

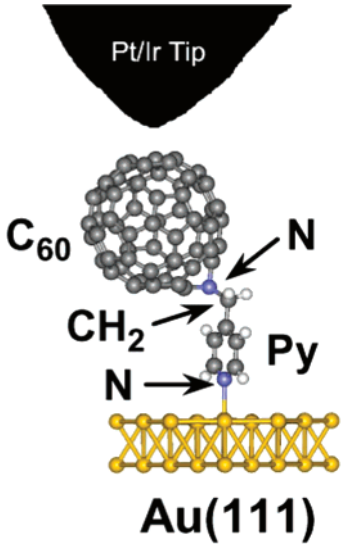

Figure 1. Schematic drawing of the model of the C_{60}NPy on Au(111) surface.

Calculations

We calculated the electronic structure of C_{60}NPy with a model shown in Figure 1 in the absence of the STM tip. With the Au surface modeled by a gold cluster consisting of 34 gold atoms, the optimized structure of the chemisorbed pyridine is found to have the nitrogen atom anchored on the top site of Au(111).[35−37] In the optimization, Au atoms in the cluster were fixed at their bulk positions except the top Au atom connected with N atom and the six Au atoms around it in the first Au layer. The N bridge connected at the 5−6 junction on C_{60} was used;[30,31,38] here we abbreviate the group as C_{60}N. All calculations were performed by the molecular simulation package DMol3,[39] which is based on the DFT method.[40−43] The PBE (Perdew, Burke, and Enzerhof) functional was chosen together with the DNP basis sets,[40] which is the double numerical atomic orbitals augmented by polarization functions. The electronic structure was obtained by solving the Kohn−Sham equations self-consistently.[41,42] All-electron calculations with scalar relativistic corrections were used. High grid mesh points were employed for the matrix integrations. Self-consistent-field procedures were done with a convergence criterion of 10^{-6} au on the energy and electron density. Geometric optimization was performed using the Broyden−Fletcher−Goldfarb−Shanno (BFGS) algorithm[43] with a convergence criterion of 10^{-3} a.u. on the gradient, 10^{-3} au on the displacement, and 10^{-5} au on the energy. We have checked the Hessian matrix and found that nearly all the eigenvalues are positive except two small negative values that may be assigned to zero within precision, indicating that our system is stable.

For comparison, we also calculated the electronic structures of the hydrogen-terminated groups of C_{60}NH and $Au_{34}-$pyridine (abbreviated as $Au_{34}-$PyH) to simulate the D part and the A part separately, where a hydrogen is used to saturate the N bond and the C bond on C_{60}N group and Py group, respectively.

Results and Discussion

STM/STS Characterization of the SAMs. *CP-SAM.* The sole assembly of C_{60}NPy only results in disordered films of C_{60}NPy even when the films were annealed at 105 °C.[34] As shown in Figure 2a, the intramolecular patterns of C_{60} moieties with random orientation can be observed. The observation of the intramolecular patterns of C_{60} indicates that the rotation of

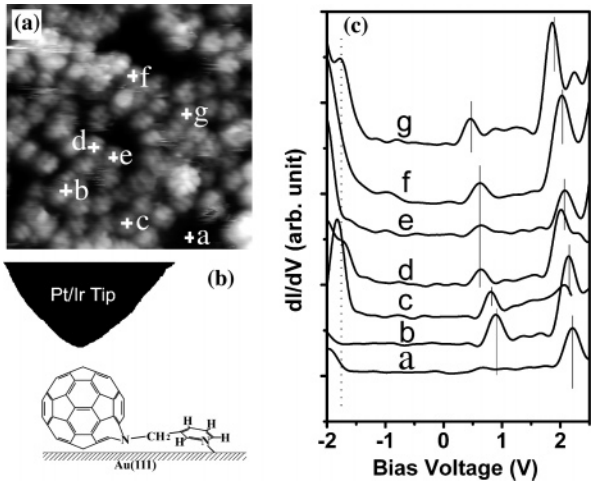

Figure 2. (a) STM image of the C_{60}NPy molecules solely assembled on bare gold substrate: scanning parameters 2.0 V and 250 pA; scanning area 12 × 12 nm^2. (b) Schematic drawing of the tip of the microscope to take $I-V$ curves over recumbent C_{60}NPy molecules by locating the tip over the C_{60} moiety. (c) Representative numerical dI/dV spectra taken at the marked sites in (a).

C_{60} is frozen.[44] The lying-down C_{60}NPy on Au(111) may result in the disordered morphology of the sole assembly of C_{60}NPy film, causing the variation in the environment of the molecules from one to another. The $I-V$ curves were taken by locating the tip of the microscope over the center of C_{60} moieties of the C_{60}NPy molecules, as the illustration shows in Figure 2b. Accordingly, several representative numerical differential dI/dV spectra taken at the marked sites of the C_{60} moieties are shown in Figure 2c. Though the $I-V$ curves or the dI/dV spectra at each sites were highly reproducible, the features in the $I-V$ curves or the dI/dV spectra varied from site to site. We may assign the site-dependent features in dI/dV spectra to the uncertain environments due to the random lying-down molecules. We note that the features shown in Figure 2c are quite similar to those for pristine C_{60} monolayer on different metal surfaces of Au(111), Ag(001), and Cu(111),[45−48] where the different electronic structures of the adsorbed C_{60} molecules mainly reflect the different interactions between the molecules and the metal surfaces. Thus, the site-dependent electronic structures shown in Figure 2c may not reflect the intrinsic transport properties of the C_{60}NPy molecules.

co-SAM-1 and co-SAM-2. Fortunately, C_{60}NPy may form quite ordered structure in co-assembled films. We have studied the topographies of the co-assembled films of BM and C_{60}NPy;[34] here we just concentrate on the topic of the electron transport behavior of the molecule. By locating the STM tip over the C_{60} moieties, as illustrated in Figure 1, we obtained quite reproducible features in $I-V$ curves (or in dI/dV spectra) at different sites of the C_{60}NPy molecules in the co-assembled films of BM and C_{60}NPy. Figure 3 shows the images of the samples of co-SAM-1 and co-SAM-2 and the $I-V$ curves taken over the positions marked in the images.

In Figure 3d, we can see that the main features in $I-V$ curves taken over the C_{60}NPy molecules (curves b, c, d, e, h, and i) are overall quite similar. These curves have positive onset voltages around 0.5 V and negative onset voltages around −1.7 V, forming asymmetric $I-V$ characteristics and giving a rectification ratio (RR) about 10 at ±1.0 V. The features obtained from the C_{60}NPy molecules are obviously different from the ones from BM and the Au substrate (curves a, f, and g). Moreover, we observe fine features in curves h and i for C_{60}NPy measured at 5 K. In contrast to curve g for the Au

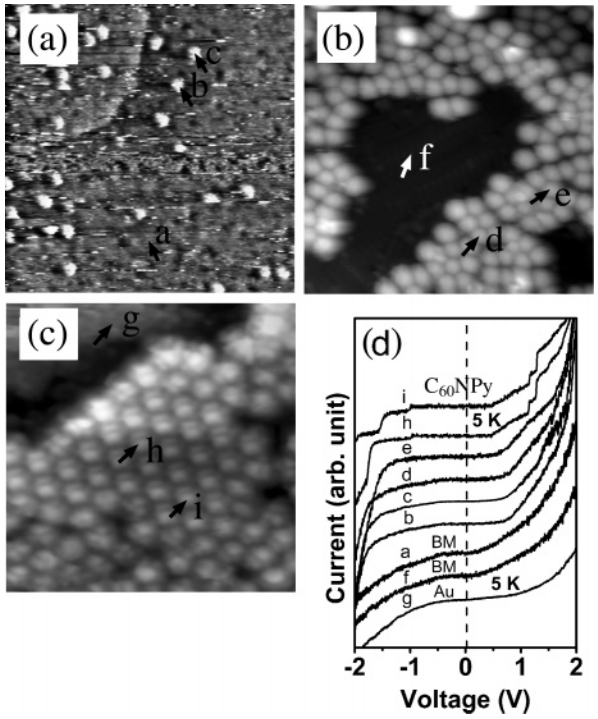

Figure 3. STM images of C_{60}NPy molecules co-assembled with BM molecules for (a) co-SAM-1 (50 × 50 nm^2), (b) co-SAM-2 (20 × 20 nm^2), and (c) co-SAM-2 annealed at 105 °C for 10 h (10 × 10 nm^2). (d) $I-V$ curves taken over the positions marked in the images at 78 K except for curves g, h, and i taken at 5 K, where curves a and f were taken over the BM SAM, curve g was taken over the gold substrate, and the left curves were taken over C_{60}NPy.The dashed line is a guide for the eye.

substrate with the same tip and the same temperature at 5 K, it is obvious that the fine features for C_{60}NPy are not due to the STM tip effects. The fine features in the $I-V$ curves for C_{60}-NPy were quite reproducible not only for the same sites, but also for different sites over the C_{60}NPy SAM (see Supporting Information).

Here, a C_{60}NPy molecule, with pyridine−σ−C_{60} oligomeric structure, forms a basic AR model of D−σ−A rectifier.[1,15,49] The C_{60} moiety participates as an electron acceptor (A), the pyridine moiety bonded to the Au substrate as an electron donor (D), and the single methylene (−CH_2−) bridge as a σ-bridge. For further discussion, we plot the $I-V$ curve h and its dI/dV spectra in Figure 4. The curve shows some clear stepwise fine features at positive voltages and less pronounced at negative voltages. The current jumps may be caused by the intramolecular resonant tunneling between the different parts of the C_{60}NPy molecules. The fine features are more clearly seen as the differential conductance peaks in the numerical dI/dV spectrum in the upper panel in Figure 4, where the dI/dV spectrum may reflect the local density of state (DOS) of an individual molecule.[44−46,50−57] Since the $I-V$ curves taken at 5 K give clearer fine features, our following discussion will be based on the results obtained at 5 K.

Does the Short σ-Bridge Decouple the LUMO and the HOMO of the Donor and the Acceptor? In an AR rectifier, the σ-bridge plays an important role in decoupling the related orbitals, especially the LUMO and the HOMO, of the donor and the acceptor for obtaining the rectifying effect. To understand whether the observed rectification in our system is attributed to the AR model, we should first check if the short σ-bridge participates as a barrier to decouple the two parts. We performed the calculation by modeling a gold cluster containing

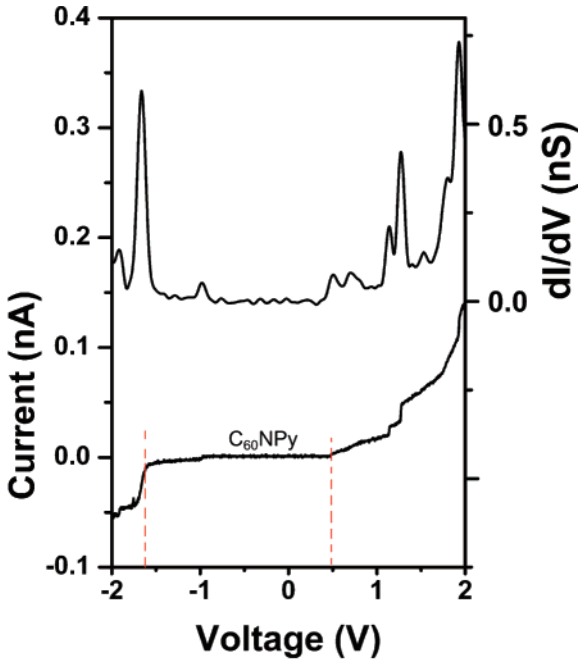

Figure 4. *I*−*V* curve and its numerical d*I*/d*V* spectrum for C_{60}NPy measured at 5 K taken at a gap voltage of 2.0 V and a set-point current of 0.2 nA. The bias voltage was applied to the gold substrate electrode.

34 atoms connected to C_{60}NPy via the Au−N bond. Such cluster models are widely used in the study of the electron transport in molecules, and may provide contact information of the molecule and the electrodes.[3,28,58−60] Here, we treat the C_{60}NPy−Au_{34} as an extended molecule.[61−66]

Figure 5 shows the calculated densities of states (DOSs) of C_{60}NPy−Au_{34}, Au_{34}−PyH, and C_{60}NH. For comparison, the partial densities of states (PDOSs) of the groups of Au_{34}−Py and C_{60}N in C_{60}NPy−Au_{34} are also shown. The DOS and the PDOS were obtained by a Lorentzian extension with a broadening width of 0.05 eV of the discrete energy levels and a summation over them. Comparing the DOSs of Au_{34}−PyH and C_{60}NH with the PDOSs of Au_{34}−Py and C_{60}N, respectively, we may see that the electronic structures of Au_{34}−PyH and C_{60}NH correspondingly resemble the ones of the groups of Au_{34}−Py and C_{60}N in the C_{60}NPy molecule fairly well, indicating overall that the orbitals either localized on the C_{60}N group or on Au_{34}−Py, except for the shifts of the peaks for C_{60}N at −1.7, −1.0, and 0.6 eV, as marked by the arrows. Here, the relative shifts of the three peaks in the case of the C_{60}NH group indicate that the H termination is not saturated enough at these energies. When C_{60}N is connected to Py via a $-CH_2-$ bridge, the wave function of the C_{60}N may extend somewhat to the bridge at these energies. As we will discuss below, the extension of the wave function at the energies may affect the electron transport of the C_{60}NPy molecule.

To see the wave function distribution on the molecule, the orbital frontiers of several related states labeled in Figure 5 are plotted in Figure 6. We may see that orbitals 2 and 3 are mainly localized on the Au_{34}−Py group, corresponding to the localized LUMO and HOMO of the donor, and orbitals 1 and 4 are mainly localized on the C_{60}N group, corresponding to the localized LUMO and HOMO of the acceptor. In this configuration, the donor's LUMO and HOMO (orbitals 2 and 3) and the acceptor's LUMO and HOMO (orbitals 1 and 4) are asymmetrically positioned with respect to the FLE, respectively. A relatively small HOMO−LUMO gap of the donor is due to the hybridization of the Py and the gold atoms.

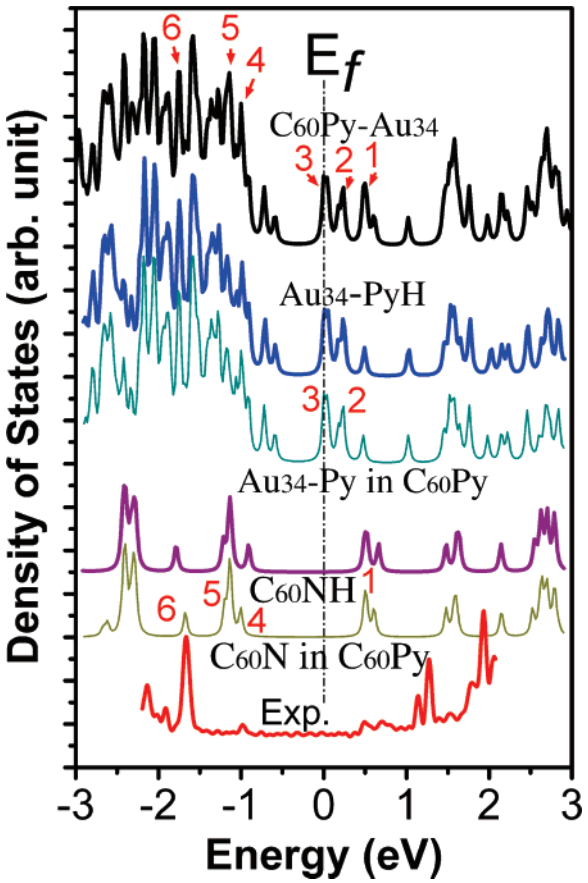

Figure 5. Calculated densities of states of C_{60}NPy−Au_{34}, Au_{34}−PyH, and C_{60}NH, compared with experimental results. The partial densities of states of the groups of Au_{34}−Py and C_{60}N in C_{60}NPy−Au_{34} are also plotted for comparison with the ones of the hydrogen-saturated groups of Au_{34}−PyH, and C_{60}NH. The energy levels are aligned to the Fermi energy with a shift of 5.15 eV. Several states related to the discussion are labeled. The dashed lines denote the level shifts when the C_{60}N is terminated by a hydrogen atom.

As it is noticed above that orbital 4 (acceptor's HOMO) at an energy of about −1.0 eV is not well saturated with H, the wave function of C_{60}N extends in a certain range to the *σ*-bridge, but not to the Py. Hence, we can see that the HOMO and the LUMO of the donor and the acceptor are overall localized on either the C_{60} moiety or the Au_{34}−Py group. Further calculations show that the LUMO and the HOMO are delocalized at −1.0 eV for the system without a methylene bridge, while the molecular obitals are well localized over the whole energy region explored for the system with a trimethylene bridge (see Supporting Information). This indicates that the *σ*-bridge in C_{60}NPy−Au_{34} plays a key role in decoupling the donor and the acceptor, at least the LUMO and the HOMO.

Details of the Electron Transport through the C_{60}NPy. The differential conductance peaks in the d*I*/d*V* spectra may offer us a clue to understanding the relevant transport mechanism. The d*I*/d*V* spectrum for C_{60}NPy is also plotted in Figure 5 to compare with the DOS of C_{60}NPy, as well as the PDOSs of C_{60}N and Au_{34}−Py. Considering the commonly existing distinction in unoccupied orbitals using DFT method, we may see that the experimental conductance peaks may find their corresponding PDOS peaks of the C_{60}N group, except for the absence of a peak at −1.1 eV. These behaviors can be understood by analyzing the electron transport through the orbitals of the donor and the acceptor of C_{60}NPy in detail.

Electron Transport between Donor and Acceptor. According to the calculated energy levels shown in Figure 5, we now

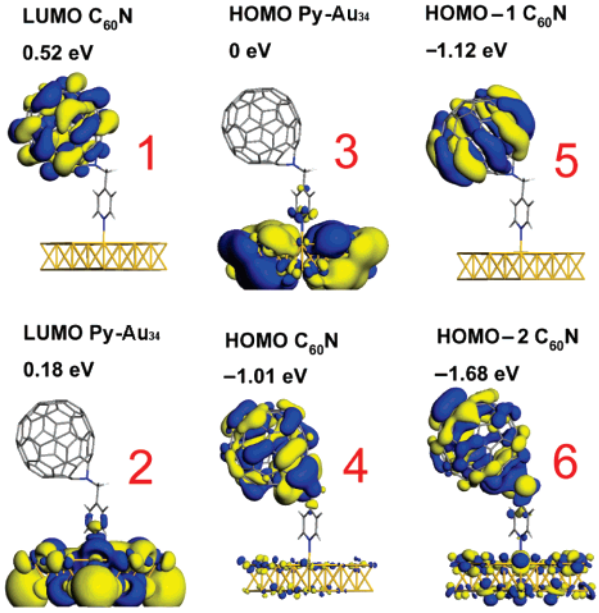

Figure 6. Orbital frontiers of absorbed C_{60}NPy on gold. Orbitals 2 and 3 are the LUMO and HOMO for Py−Au_{34}, 1 and 4 are the LUMO and HOMO for C_{60}N, and 5 and 6 are the HOMO−1 and HOMO−2 for C_{60}N, respectively.

discuss how the current flows through C_{60}NPy. As illustrated in Figure 7a for forward bias applied, once the applied voltage becomes large enough for the Fermi level of the STM tip to be aligned with or higher than the acceptor orbital 1, electron tunneling onto the acceptor orbital 1 occurs. Consequently, the additional electron on orbital 1 further tunnels inelastically onto donor orbital 2 or 3; here the tunneling from orbital 1 to orbital 3 may occur only when the electron transfer from orbital 3 onto the gold electrode occurs. Then, the current flow through C_{60}-NPy is observed. This corresponds to the first current step at positive voltage in the $I-V$ characteristic (or the peak in dI/dV spectrum). As shown in Figure 5, the positive onset voltage is 0.5 V, which is well coincident to the calculated LUMO energy of 0.5 eV for the acceptor. With further increase of the voltage, the FLE may align the higher acceptor orbitals, opening up additional current channels. With every additional transport channel, the current grows by a certain amount, resulting in a stepwise increase in the $I-V$ (or a peak in the differential conductance dI/dV), similar to the observations by Elbing et al.[6] However, we measured at a much lower temperature than Elbing et al. did; hence, the $I-V$ curves gave sharper steps.

For the reverse bias applied, as shown in Figure 7b, a similar process may occur when the Fermi level of the STM tip is aligned with or lower than the acceptor HOMO orbital 4. In the process, an electron tunnels from orbital 4 onto the STM tip, and then a hole forms on orbital 4. Consequently, electrons on the donor orbital 3 may tunnel onto orbital 4, following the electron transfer from the gold electrode onto orbital 3. Thus, current flow at reverse bias occurs, corresponding to the first current step at negative voltage. Here, the first current step occurs at −1.0 V, well coincident to the HOMO energy of −1.0 eV for the acceptor. Further lowering the Fermi level of the STM tip may also open up additional current channels at negative voltages.

One may note that the energy levels illustrated in Figure 7a,b nearly do not shift between the donor and the acceptor with forward and reverse applied voltages. As shown in the contour images in Figure 7c,d and the discussion below, there is no shift between the energy levels for the donor and the acceptor because the applied voltage mainly drops over the vacuum gap, but a small fraction of the voltage drops over the molecule itself. Here, parts c and d of Figure 7 show the calculated results of the difference of the electrostatic potentials with an electric field of 0.001 au along the molecule and without an electric field at positive and negative bias, respectively, reflecting that the voltage mainly drops over the vacuum junction.

Negative and Positive Onset Voltages. The negative and positive onset voltages, as well as the RR value, are of great concern in a molecular rectifier. These parameters are determined by the contributions of molecular orbitals to the current. Results by Heurich et al. showed that the transport properties of molecules may not be dominated by the LUMO and the HOMO.[62] Rather, several factors, such as the bridging extent, the energy position of an orbital, and the coupling of the molecule to the electrodes, may determine the contribution of the orbital to the current. Based on this analysis, it is easy to understand the negative onset voltage of −1.7 V since orbital 6 at an energy of around −1.7 eV extends to the whole molecule, including the electrode. This indicates that, at energy of −1.7 eV, the short σ-bridge may not be as a good barrier as it is at the energies of the LUMO and HOMO. Our calculation shows that a trimethylene bridge may decouple the donor and the acceptor better than a single methylene bridge.

Due to the relatively small LUMO−HOMO gap for the donor, and the donor HOMO (orbital 3) close to the Fermi energy, once the Fermi level of the STM tip is aligned with or higher (lower) than the LUMO (HOMO) of the acceptor at a certain bias, it is possible to have the current flow between the two electrodes. The behaviors in our observations meet the predicted condition of a small gap between the HOMO of the donor and the LUMO of the acceptor for rectification.[28] As discussed above, when the applied bias voltage reaches 0.5 V, the FLE of the PtIr tip may match the acceptor LUMO of 0.5 eV since the voltage mainly drops over the vacuum junction; thus, it opens up the first current channel. When the voltage is higher than 0.5 V, the relatively quick increase of the current may be contributed by those orbitals that span the molecule and the electrode, and even the tails of the orbitals.[62]

There is only a tiny current step at −1.0 V (see Figure 4). This current step may be assigned to the contribution of orbital 4 of −1.0 eV (see Figure 5). The very close orbital 5 does not contribute to the current. This can be understood by considering the coupling of the molecule to the electrode. At energies of −1.0 and −1.1 eV, orbitals 4 and 5 are well confined to C_{60}N and their weight at the gold atoms is very small, especially that of orbital 5. Thus, according to the judgment of Heurich et al.,[62] the two orbitals may not significantly contribute to the current.

The rectification ratio of about 10 at ±1.0 V observed in our system falls into the typical RR range of 2−30 at ±1.0 V obtained in other systems.[3,8,17−21,67−75] In those systems, the molecular origin of the electrical asymmetry has been verified.[4,17,19−21,67,68] Very recently, much higher rectification ratios in excess of 100[4,6,76] and the highest to date of 3000 at ±1.0 V in the systems of cationic D−π−A^+ dyes coupled with anionic donors have been reported.[6] The chromophores either asymmetrically contacted the electrodes[8,10,73] or nearly symmetrically contacted the electrodes,[6,17−21,75,76] where the D−bridge−A unit was not dispensable.

Aspects of Voltage Drops over the Molecular Junction. As we have discussed above, the applied voltage mainly drops over the vacuum gap. Here, we may estimate the voltage drop of the molecular junction. The total resistance of the molecular junction is estimated to be about 10 GΩ at the gap voltage of

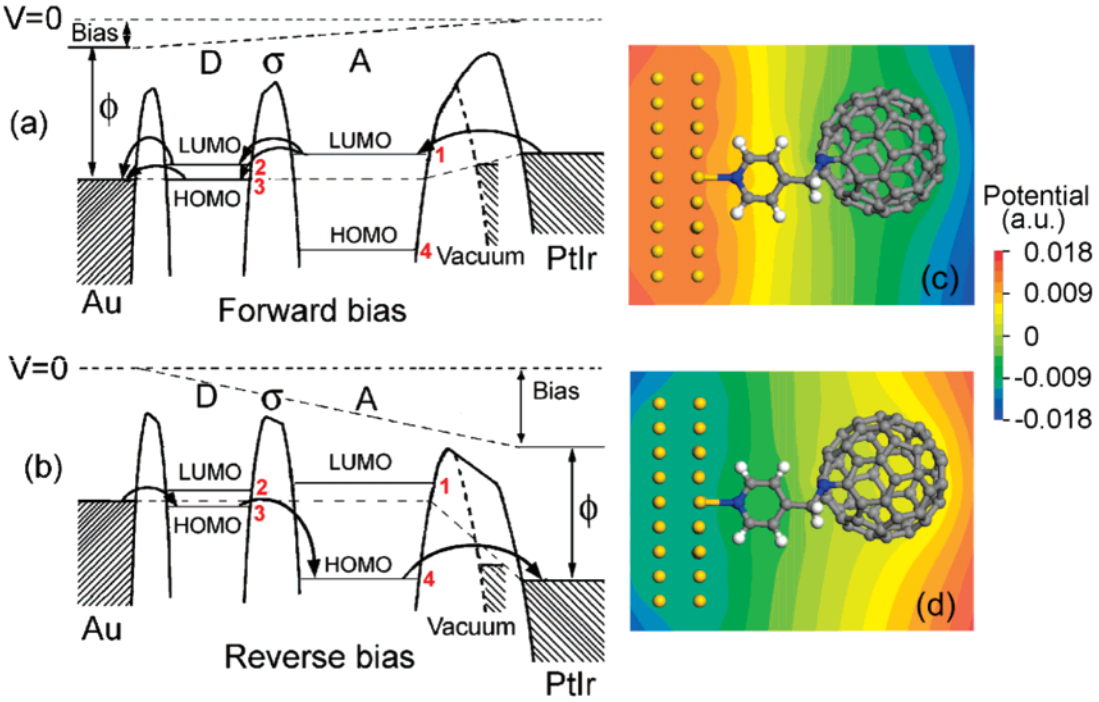

Figure 7. Schematic drawings of the electron transport in C_{60}NPy for (a) forward bias and (b) reverse bias. The vacuum barriers in dashed lines denote the barriers at a higher feedback current. Calculated voltage drop on the molecule for (c) forward bias and (d) reverse bias. The data are obtained by calculating the difference of the electrostatic potentials with an electric field of 0.001 au along the molecule and without an electric field.

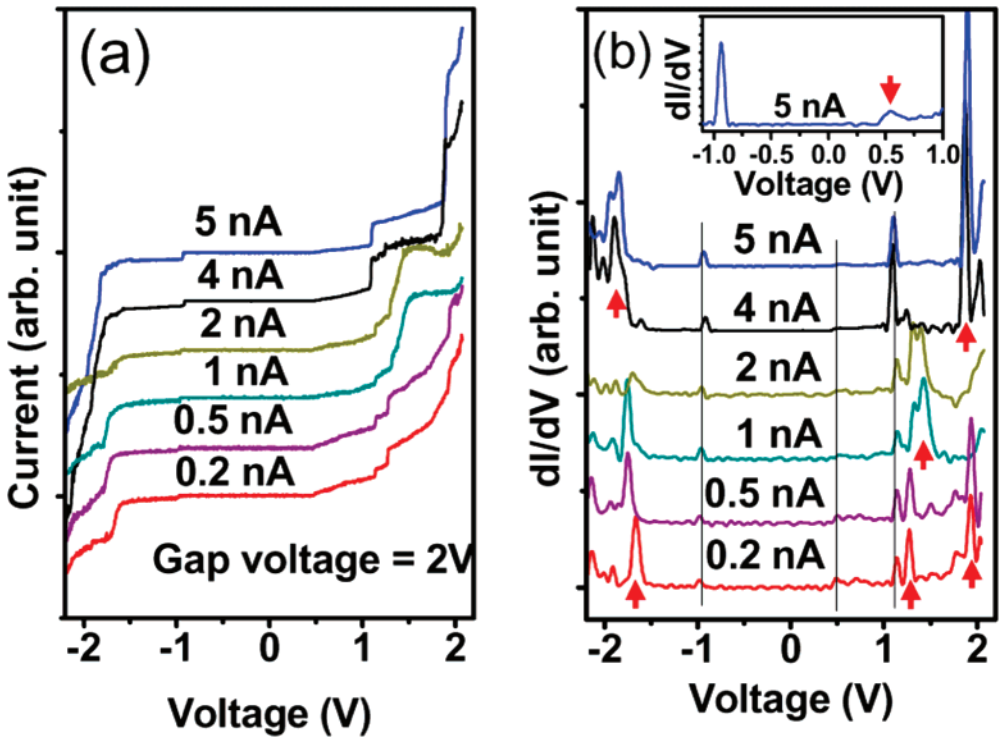

Figure 8. (a) $I-V$ curves and (b) their dI/dV spectra at gap voltage of 2 V and various feedback currents (labeled on the curves) taken at 5 K. The inset shows the relatively weak peak around 0.5 V for the spectrum taken at feedback current of 5 nA.

2.0 V and feedback current of 0.2 nA of the STM. Since we lack the resistance value of C_{60}NPy, we adopt a value of 50 MΩ for octanedithiol,[77] which has a length similar to that of C_{60}NPy, as an upper limit resistance value for C_{60}NPy. Compared with the resistance of about 10 GΩ of the molecular junction, the molecule has very small resistance, so the voltage drop on the molecule itself may be neglected, and the voltage almost drops over the tip−molecule vacuum junction.

When the feedback current changes from 0.2 to 5 nA, the vacuum gap between the tip and the molecule is reduced, as illustrated by the vacuum barriers in the dashed lines in Figure 7a,b. This causes the decrease of the impedance of the molecular junction by a factor of about 25 from 10 GΩ to 400 MΩ. Though we expect the increasing of the voltage drop over the molecule, the amount still remains small. Compared to the resistance of the molecule, 50 MΩ, the voltage drop over the

vacuum gap is still larger by a factor of 7 than the drop over the molecule at the feedback current of 5 nA. Then, the $I-V$ characteristics or the differential dI/dV of the molecular junction should remain. These behaviors have been confirmed, as shown in Figure 8, by the three unchanged steps or the peaks located around −1.0, 0.5, and 1.1 eV. At higher voltages in the dI/dV spectra, we may observe a peak shift or disappearance at a certain feedback current, which may involve some complex effects of applied field, and we do not discuss that here.

Here, we suggest that the voltage drop on the molecule−electrode interfaces may not consequentially result in the absence of the rectification in a molecular junction, in contrast to the suggestion by Mujica et al.[24] Instead, the voltage drop on the interfaces may be helpful to maintain the rectification as long as the asymmetric energy level configuration exists. The role of the vacuum gap in our system is somewhat similar to those of the tailored alkyl chains in other molecular systems.[6,11,15,17−21,23,75,76] When the voltage mainly drops over the vacuum gap, it is helpful for the Fermi energy of the electrode sweeping over the levels of the molecules. The determination of the rectifying effect is the asymmetric configuration of the obitals rather than the interfaces, as discussed by Krzeminski et al.[16] However, due to a small voltage drop over the molecule, the levels' shift between the acceptor and the donor should be small, and thus a narrow HOMO−LUMO gap is helpful to make sure the current channels open up at appropriate voltages.[28]

When the tip got closer to the molecule (the feedback current increased), as shown in Figure 8a, the behavior of asymmetric $I-V$ characteristics was less pronounced. Since C_{60} tends to have a strong interaction with metal, with accompanying charge transfer between them,[45−48] the less asymmetric $I-V$ behavior may be easily assigned at higher feedback current to the interaction between the tip and the C_{60}. However, considering that the tip was still far enough to take the image clearly, we believe the tip−molecule junction is still in tunneling regime. Moreover, the remaining peak positions at higher feedback current also indicate there is no obvious electron transfer. Therefore, the C_{60}−tip interaction can be neglected even at a feedback current of 5 nA. If the current jumps may be attributed to intramolecular resonant tunneling, the enhanced current jumps (or conductance peaks) in Figure 8 may be assigned due to the fact that the resonant condition is approached between the different parts of the molecule at higher feedback current. A better designed molecular device needs to consider such an electric-field-dependent effect on electron transport.

Conclusions

In conclusion, we studied the electron transport of single C_{60}-NPy molecules on gold surfaces with STM. The $I-V$ curves for single C_{60}NPy molecules show asymmetric features, i.e., rectification at a single molecular scale. The positive onset voltage is 0.5 V, and the negative onset voltage is −1.7 V. Their differential dI/dV spectra give fine conductance peaks measured at 5 K, which can be directly compared with the calculated DOS of C_{60}NPy chemically adsorbed on Au substrate based on the DFT method. The analysis shows that the rectifying effect is assigned to the asymmetric energy levels of the C_{60}NPy molecules with respect to the FLE. In principle, the electron transport through a single C_{60}NPy molecule accords well with the AR rectifiers, which indicates that the rectifier in the molecular architecture of D−σ−A works at a single molecular scale. However, our experimental results also show that the asymmetric geometric junction is also helpful for rectifying. The existence of the relatively long alkyl chain causes the major drop of the applied voltage over the separating part of the alkyl chain, but a small fractional drop of the voltage over the D−σ−A group. Hence, in this situation, the level shifts between the A and the D parts should be small, and a narrow HOMO−LUMO gap is necessary to make sure the current channels open up at appropriate voltages.

Acknowledgment. We thank Prof. Y. L. Li from the Institute of Chemistry of CAS for his help in the synthesis of the molecules. This work is supported by the NPDKFSC (G2001CB3095), by the NSFC (50121202, 10374083, 10474088, 20473077, 50532040), and by NCET-04-0579.

Supporting Information Available: Details of the sample preparation; several $I-V$ curves taken at different points; comparison of calculations for C_{60}NPy with a trimethylene bridge, a single methylene bridge, and without methylene; comparison of the images for the pure BM SAM and the co-assembled SAM of BM and C_{60}NPy. This material is available free of charge via the Internet at http://pubs.acs.org.

References and Notes

(1) Aviram, A.; Ratner, M. A. *Chem. Phys. Lett.* **1974**, *29*, 277.
(2) Zhao, J.; Zeng, C. G.; Cheng, X.; Wang, K. D.; Wang, G. W.; Yang, J. L.; Hou, J. G.; Zhu, Q. S. *Phys. Rev. Lett.* **2005**, *95*, 045502.
(3) Elbing, M.; Ochs, R.; Koentopp, M.; Fischer, M.; von Hanisch, C.; Weigend, F.; Evers, F.; Weber, H. B.; Mayor, M. *Proc. Natl. Acad. Sci. U.S.A.* **2005**, *102*, 8815.
(4) Ashwell, G. J.; Mohib, A. *J. Am. Chem. Soc.* **2005**, *127*, 16238.
(5) Morales, G. M.; Jiang, P.; Yuan, S. W.; Lee, Y. G.; Sanchez, A.; You, W.; Yu, L. P. *J. Am. Chem. Soc.* **2005**, *127*, 10456.
(6) Ashwell, G. J.; Urasinska, B.; Tyrrell, W. D. *Phys. Chem. Chem. Phys.* **2006**, *8*, 3314.
(7) Metzger, R. M.; Chen, B.; Hopfner, U.; Lakshmikantham, M. V.; Vuillaume, D.; Kawai, T.; Wu, X. L.; Tachibana, H.; Hughes, T. V.; Sakurai, H.; Baldwin, J. W.; Hosch, C.; Cava, M. P.; Brehmer, L.; Ashwell, G. J. *J. Am. Chem. Soc.* **1997**, *119*, 10455.
(8) Metzger, R. M.; Xu, T.; Peterson, I. R. *J. Phys. Chem. B* **2001**, *105*, 7280.
(9) Martin, A. S.; Sambles, J. R.; Ashwell, G. J. *Phys. Rev. Lett.* **1993**, *70*, 218.
(10) Ho, G.; Heath, J. R.; Kondratenko, M.; Perepichka, D. F.; Arseneault, K.; Pezolet, M.; Bryce, M. R. *Chem.—Eur. J.* **2005**, *11*, 2914.
(11) Metzger, R. M.; Baldwin, J. W.; Shumate, W. J.; Peterson, I. R.; Mani, P.; Mankey, G. J.; Morris, T.; Szulczewski, G.; Bosi, S.; Prato, M.; Comito, A.; Rubin, Y. *J. Phys. Chem. B* **2003**, *107*, 1021.
(12) Zhou, C.; Deshpande, M. R.; Reed, M. A.; Jones, L.; Tour, J. M. *Appl. Phys. Lett.* **1997**, *71*, 611.
(13) Liu, Y. Q.; Xu, Y.; Zhu, D. B. *Synth. Met.* **1997**, *90*, 143.
(14) Chabinyc, M. L.; Chen, X. X.; Holmlin, R. E.; Jacobs, H.; Skulason, H.; Frisbie, C. D.; Mujica, V.; Ratner, M. A.; Rampi, M. A.; Whitesides, G. M. *J. Am. Chem. Soc.* **2002**, *124*, 11730.
(15) Metzger, R. M. *Chem. Rec.* **2004**, *4*, 291.
(16) Krzeminski, C.; Delerue, C.; Allan, G.; Vuillaume, D.; Metzger, R. M. *Phys. Rev. B* **2001**, *64*, 085405.
(17) Ashwell, G. J.; Chwialkowska, A.; High, L. R. H. *J. Mater. Chem.* **2004**, *14*, 2848.
(18) Ashwell, G. J.; Mohib, A.; Miller, J. R. *J. Mater. Chem.* **2005**, *15*, 1160.
(19) Ashwell, G. J.; Hamilton, R.; High, L. R. H. *J. Mater. Chem.* **2003**, *13*, 1501.
(20) Ashwell, G. J.; Chwialkowska, A.; High, L. R. H. *J. Mater. Chem.* **2004**, *14*, 2389.
(21) Ashwell, G. J.; Tyrrell, W. D.; Whittam, A. J. *J. Am. Chem. Soc.* **2004**, *126*, 7102.
(22) Geddes, N. J.; Sambles, J. R.; Jarvis, D. J.; Parker, W. G.; Sandman, D. J. *Appl. Phys. Lett.* **1990**, *56*, 1916.
(23) Brady, A. C.; Hodder, B.; Martin, A. S.; Sambles, J. R.; Ewels, C. P.; Jones, R.; Briddon, P. R.; Musa, A. M.; Panetta, C. A. F.; Mattern, D. L. *J. Mater. Chem.* **1999**, *9*, 2271.
(24) Mujica, V.; Ratner, M. A.; Nitzan, A. *Chem. Phys.* **2002**, *281*, 147.
(25) Ellenbogen, J. C.; Love, J. C. *Proc. IEEE* **2000**, *88*, 386.
(26) Datta, S.; Tian, W. D.; Hong, S. H.; Reifenberger, R.; Henderson, J. I.; Kubiak, C. P. *Phys. Rev. Lett.* **1997**, *79*, 2530.
(27) Pickholz, M.; dos Santos, M. C. *THEOCHEM* **1998**, *432*, 89.
(28) Stokbro, K.; Taylor, J.; Brandbyge, M. *J. Am. Chem. Soc.* **2003**, *125*, 3674.

(29) Salomon, A.; Cahen, D.; Lindsay, S.; Tomfohr, J.; Engelkes, V. B.; Frisbie, C. D. *Adv. Mater.* **2003**, *15*, 1881.
(30) Prato, M.; Li, Q. C.; Wudl, F.; Lucchini, V. *J. Am. Chem. Soc.* **1993**, *115*, 1148.
(31) Prato, M.; Lucchini, V.; Maggini, M.; Stimpfl, E.; Scorrano, G.; Eiermann, M.; Suzuki, T.; Wudl, F. *J. Am. Chem. Soc.* **1993**, *115*, 8479.
(32) Alvarez, S. G.; Alvarez, M. T. *Synthesis* **1997**, 413.
(33) Wu, Y.; Ahlberg, P. *J. Org. Chem.* **1992**, *57*, 6324.
(34) Zhou, Y. S.; Wang, K. D.; Zhao, F. Z.; Wang, B.; Hou, J. G.; Wang, S.; Li, Y. L. *Chin. Sci. Bull.* **2005**, *50*, 406.
(35) Wu, X. J.; Li, Q. X.; Huang, J.; Yang, J. L. *J. Chem. Phys.* **2005**, *123*, 184712.
(36) Hou, S. M.; Zhang, J. X.; Li, R.; Ning, J.; Han, R. S.; Shen, Z. Y.; Zhao, X. Y.; Xue, Z. Q.; Wu, Q. *Nanotechnology* **2005**, *16*, 239.
(37) Bilic, A.; Reimers, J. R.; Hush, N. S. *J. Phys. Chem. B* **2002**, *106*, 6740.
(38) Our calculation shows that the configurations of Py tailored through CH_2-N at 5−6 junction and 6−6 junction on C_{60} give similar results.
(39) DMol3 is a density-functional-theory-based package with atomic basis distributed by Accelrys [Delly, B. *J. Chem. Phys.* **1990**, *92*, 508−517].
(40) Perdew, J. P.; Burke, K.; Ernzerhof, M. *Phys. Rev. Lett.* **1996**, *77*, 3865.
(41) Hohenberg, P.; Kohn, W. *Phys. Rev.* **1964**, *136*, B864.
(42) Kohn, W.; Sham, L. J. *Phys. Rev.* **1965**, *140*, A1133.
(43) Fletcher, R. *Practical Methods of Optimization*; Wiley: New York, 1980; Vol. 1.
(44) Wang, H. Q.; Zeng, C. G.; Li, Q. X.; Wang, B.; Yang, J. L.; Hou, J. G.; Zhu, Q. S. *Surf. Sci.* **1999**, *442*, L1024.
(45) Lu, X. H.; Grobis, M.; Khoo, K. H.; Louie, S. G.; Crommie, M. F. *Phys. Rev. Lett.* **2003**, *90*, 096802.
(46) Lu, X. H.; Grobis, M.; Khoo, K. H.; Louie, S. G.; Crommie, M. F. *Phys. Rev. B* **2004**, *70*, 115418.
(47) Silien, C.; Pradhan, N. A.; Ho, W.; Thiry, P. A. *Phys. Rev. B* **2004**, *69*, 115434.
(48) Grobis, M.; Lu, X.; Crommie, M. F. *Phys. Rev. B* **2002**, *66*, 161408.
(49) Segura, J. L.; Martin, N.; Guldi, D. M. *Chem. Soc. Rev.* **2005**, *34*, 31.
(50) Wiesendanger, R. *Scanning Probe Microscopy and Spectroscopy*; Cambridge University Press: Cambridge, U.K., 1994.
(51) Feenstra, R. M.; Stroscio, J. A.; Fein, A. P. *Surf. Sci.* **1987**, *181*, 295.
(52) Hou, J. G.; Wang, B.; Yang, J. L.; Wang, K. D.; Lu, W.; Li, Z. Y.; Wang, H. Q.; Chen, D. M.; Zhu, Q. S. *Phys. Rev. Lett.* **2003**, *90*, 246803.
(53) Wang, B.; Wang, K. D.; Lu, W.; Wang, H. Q.; Li, Z. Y.; Yang, J. L.; Hou, J. G. *Appl. Phys. Lett.* **2003**, *82*, 3767.
(54) Li, B.; Zeng, C. G.; Li, Q. X.; Wang, B.; Yuan, L. F.; Wang, H. Q.; Yang, J. L.; Hou, J. G.; Zhu, Q. S. *J. Phys. Chem. B* **2003**, *107*, 972.
(55) Zeng, C. G.; Li, B.; Wang, B.; Wang, H. Q.; Wang, K. D.; Yang, J. L.; Hou, J. G.; Zhu, Q. S. *J. Chem. Phys.* **2002**, *117*, 851.
(56) Wang, B.; Wang, K. D.; Lu, W.; Yang, J. L.; Hou, J. G. *Phys. Rev. B* **2004**, *70*, 205411.
(57) Wang, K. D.; Zhao, J.; Yang, S. F.; Chen, L.; Li, Q. X.; Wang, B.; Yang, S. H.; Yang, J. L.; Hou, J. G.; Zhu, Q. S. *Phys. Rev. Lett.* **2003**, *91*, 185504.
(58) Geng, H.; Yin, S. W.; Chen, K.-Q.; Shuai, Z. G. *J. Phys. Chem. B* **2005**, *109*, 12304.
(59) Brandbyge, M.; Kobayashi, N.; Tsukada, M. *Phys. Rev. B* **1999**, *60*, 17064.
(60) Brandbyge, M.; Mozos, J.-L.; Ordejon, P.; Taylor, J.; Stokbro, K. *Phys. Rev. B* **2002**, *65*, 165401.
(61) Seminario, J. M.; De La Cruz, C.; Derosa, P. A.; Yan, L. M. *J. Phys. Chem. B* **2004**, *108*, 17879.
(62) Heurich, J.; Cuevas, J. C.; Wenzel, W.; Schon, G. *Phys. Rev. Lett.* **2002**, *88*, 256803.
(63) Seminario, J. M.; Zacarias, A. G.; Derosa, P. A. *J. Phys. Chem. A* **2001**, *105*, 791.
(64) Seminario, J. M.; Zacarias, A. G.; Derosa, P. A. *J. Chem. Phys.* **2002**, *116*, 1671.
(65) Seminario, J. M.; Zacarias, A. G.; Tour, J. M. *J. Phys. Chem. A* **1999**, *103*, 7883.
(66) Seminario, J. M.; Zacarias, A. G.; Tour, J. M. *J. Am. Chem. Soc.* **2000**, *122*, 3015.
(67) Ashwell, G. J.; Tyrrell, W. D.; Whittam, A. J. *J. Mater. Chem.* **2003**, *13*, 2855.
(68) Ashwell, G. J.; Robinson, B. J.; Amiri, M. A.; Locatelli, D.; Quici, S.; Roberto, D. *J. Mater. Chem.* **2005**, *15*, 4203.
(69) Ashwell, G. J.; Gandolfo, D. S. *J. Mater. Chem.* **2002**, *12*, 411.
(70) Ashwell, G. J.; Gandolfo, D. S. *J. Mater. Chem.* **2001**, *11*, 246.
(71) Baldwin, J. W.; Amaresh, R. R.; Peterson, I. R.; Shumate, W. J.; Cava, M. P.; Amiri, M. A.; Hamilton, R.; Ashwell, G. J.; Metzger, R. M. *J. Phys. Chem. B* **2002**, *106*, 12158.
(72) Ashwell, G. J.; Amiri, M. A. *J. Mater. Chem.* **2002**, *12*, 2181.
(73) Xu, T.; Peterson, I. R.; Lakshmikantham, M. V.; Metzger, R. M. *Angew. Chem., Int. Ed.* **2001**, *40*, 1749.
(74) Okazaki, N.; Sambles, J. R.; Jory, M. J.; Ashwell, G. J. *Appl. Phys. Lett.* **2002**, *81*, 2300.
(75) Honciuc, A.; Jaiswal, A.; Gong, A.; Ashworth, H.; Spangler, C. W.; Peterson, I. R.; Dalton, L. R.; Metzger, R. M. *J. Phys. Chem. B* **2005**, *109*, 857.
(76) Ashwell, G. J.; Chwialkowska, A. *Chem. Commun.* **2006**, 1404.
(77) Xu, B. Q.; Xiao, X. Y.; Tao, N. J. *J. Am. Chem. Soc.* **2003**, *125*, 16164.